Research Article

SOHAG JOURNAL OF SCIENCES

https://doi.org/10.21608/sjsci.2024.325517.1224

Design, synthesis, structural elucidation of novel Iron (III) complex based on tetra-dentate azomethine ligand: biological evaluation and molecular docking approach

Ahmed M. Abu-Dief [1,2*], Mona M. A. Alharas [1], Samir A. Abdel-Latif [3], Rafat M. El-Khatib [1]

[1] *Department of Chemistry, Sohag University, Faculty of Science, Sohag, 82524, Egypt*
[2] *Chemistry Department, College of Science, Taibah University, P.O. Box 344, Madinah, Saudi Arabia*
[3] *Department of Chemistry, Faculty of Science, Helwan University, 11795 Cairo, Egypt*
[*] *Email: ahmedabudief@science.sohag.edu.eg*

Received: 2nd October 2024, **Revised:** 19th December 2024, **Accepted:** 28th December 2024.
Published online: 31st January 2025

Abstract: Several physicochemical techniques were used to evaluate structural analysis of Fe(III) complex derived from {3,4-Bis-[(3-ethoxy-2-hydroxy-benzylidene)-amino]-phenyl}-phenyl-methanone (L ligand). The methods encompassed theoretical investigations as well as elemental analysis (CHN), conductivity, magnetic susceptibility, spectroscopic (IR, NMR, mass spectrometry), decomposition point determination, and UV-Vis spectrum analysis. In fresh DMSO solutions, molar conductance measurements showed that the Fe (III) complex is non-electrolytes, with conductance value 11.45 Ω^{-1} cm^2 mol^{-1}, IR spectra suggested that the ligand coordinates through the metal ions in a tetra-dentate fashion, utilizing the (N&O) donor sites from the (C=N&C-O) groups in the ligand moiety. Job's approach and analytical results from solution complexation indicated a molar ratio of 1:1 for the metal to ligand. In accordance with the value of the stability constant (Kf), the complex's stability order was ascertained. According to the pH profile, the compound under study is stable over a broad pH range, usually between (pH= 4:10). The geometric structures of the complex and the ligand coordination abilities were inferred with the aid of magnetic and electronic spectrum studies. The electronic structures of the investigated ligand and its complex is analyzed using quantum chemical calculations via the DFT approach. The [B3LYP] level, [B3LYP/6/311G**] degree of the unbound ligand, In the density function theory (DFT) computations, the complex' and [B3LYP/6/311G**/LANL2DZ] functional categories were employed. The results showed that the DFT calculations agree with the experimental results. Hyper conjugative interactions, molecule stability, bond strength, and intramolecular charge transfer were all studied using natural bond orbital (NBO) analysis. By computing the hyperpolarizability (β) and molecular polarizability (α) parameters, the synthesized chemical revealed various unexpected optical features that were explored in relation to its nonlinear optical properties. The anti-pathogenic activity of the generated materials was experimentally proven against a subset of gram (+) and gram (-) bacteria and several fungi using the agar well diffusion method. Additionally, the ability of the L ligand and its metal chelate to cause harm to cells of the liver, breast, and colon was investigated. Furthermore, the examined compounds' ability to suppress the DPPH radical was examined. In addition, docking of molecule simulations was finished to ascertain the mechanism by which the produced compounds bound to the intended protein binding sites.

Keywords: Imine; metal chelate; anti-pathogenic activity; cytotoxicity; DPPH inhibition.

1. Introduction

Imine ligands are extremely important due to their stability, chelating capabilities, and biological application [1]. The complexes formed by transition metal ions with Schiff bases have received a lot of attention in this research since the foundation of these ligands is made up of donor atoms that are nitrogen and oxygen [2-4]. Because of their antibacterial qualities, imine ligands with halogen groups and their metal complexes are of particular interest [5]. Furthermore, salicylaldehyde derivatives containing one or more halo atoms in the aromatic ring have been shown to exhibit biological properties suchas antifungal, anticancer, and antibacterial properties [6–10]. Metal-based medications have become substantially more significant in the medical world in recent years. They are used as medications to treat cardiovascular disease, diabetes, cancer, and inflammation [11–13]. Certain imine ligands and their transition metal complexes have also been employed as antiviral, antitubercular, fungicidal, and bactericidal medications [14–16]. The metal's activity is increased by the steric and electronic impacts of substituents in the coordination zone. Other groups on ligands that are not coordinated may also have an effect on this activity [17]. Iron (III) complexes with tetra-dentate azomethine ligands are gaining interest in biomedical applications due to their structural versatility, stability, and potential for interaction with biological systems. These complexes are often derived from Schiff base ligands (a type of azomethine ligand) and can exhibit various properties, such as catalytic activity, redox behavior, and biological activity, making them useful in several biomedical contexts. Iron (III) complexes with

azomethine ligands are used in oxidation reactions, including those mimicking enzyme functions (metalloproteins like catalase and peroxidase). Due to the abundance of iron in biological systems, such complexes are often studied to understand how natural iron-based enzymes work.

Thus, encouraged by the developments previously mentioned, here we describe our freshly L {3,4-Bis-[(3-ethoxy-2-hydroxy-benzylidene)-amino]-phenyl}-phenyl-methanone} imine ligand. The named imine ligand's composition was examined by ^{1}H (nuclear magnetic resonance), ^{13}C (nuclear magnetic resonance), IR, UV–Vis. Then its FeL complex was synthesized from the reactions of ligand with Iron (III) nitrate nonahydrate Fe $(NO_3)_3.9H_2O$ and thorough analysis of spectrum features was conducted. In fact, the biological function of the processed L imine ligand and its complex was tested versus specific types of fungus and germs. Additionally, the cytotoxic action of the ready-made imine complex was verified by docking experiments and evaluated against several cell types. Furthermore, aim of the present work includes investigating its stability, reactivity, and biological effects, with the ultimate goal of understanding the relationship between metal-ligand interactions and biological efficacy for possible future use in therapeutic applications.

2. Experimental

2.1. Reagents

Since every chemical and solvent utilized in the investigation was of the commercial reagent grade, no additional purification procedures were required. First supplies purchased from Sigma-Aldrich comprised 3-ethoxysalicyldehyde, 3, 4-diaminobenzophenone, and metal salts such Iron (III) nitrate nonahydrate Fe $(NO_3)_3.9H_2O$). Apart from that, organic solvents such concentrated HCl, glacial acetic acid, and spectroscopic grade ethanol are used. 99.9% of the acetone, piperidine, and alcohol belonged to Sigma-Aldrich.

2.2. Synthesis of L imine ligand

The condensation process includes the following steps that resulted in the production of the tetra dentate L imine ligand (see Scheme 1): - 5 mmole (1.06 g) of 3, 4-diaminobenzophenone was combined with 10 mmole (1.67 g) of 3-ethoxysalisaldhyde that had been dissolved in 100 milliliters of ethanol to create an ethanolic solution. After that, the reaction mixtures were refluxed for two hours at 85 °C while being constantly stirred. Then let it cool until a precipitate that was dark orange started to form. TLC was used to track the reaction mixture's completion. The products that had been isolated were filtered, dried over anhydrous $CaCl_2$, and then given an ethanol wash.

^{1}H NMR (d, ppm), in DMSO-d^6: δ = 1.38 (s, 6H, CH_3), 4.12 (d, 4H, CH_2), 6H, H (d, 2H, H-6,6*), 6.89(d, 2H, H-7,7*), 7.11 (d, 2H, H-8,8*), 7.33 (d, 1H, H-2,2*), 7.67(s,2H,H-1,1*), 7.46 (d, 1H, H-5), 7.5 (d, 1H, H-3), 8.89 (s, 2CH=N). 12.35 ppm (s, 2H/ -OH), ^{13}C NMR for L (Figure S1), δ = 14.3 (CH_3), 65.4 (CH_2), 117.9 (CH), 119.0 (Cq), 121.8 (CH), 122.0 (CH), 123.0(CH), 124.9(CH), 128.2 (CH), 129.9(CH)130.1 (CH), 132.2 (CH), 137.6 (Cq),163.7ppm (CH=N).

2.3. Preparation of FeL imine complex

The Fe (III) imine complex was obtained by following a conventional protocol: A molar ratio of 1:1 was observed when 10 mmol of L imine ligand (4.49 g) was diluted with ethanol and 10 mmol of Fe $(NO_3)_3.9H_2O$ metallic salt (4.04 g) was dissolved in an aqueous ethanolic mixture. After refluxing for an hour at 85 °C, we add a drop of Piperidine. about half an hour later the complex's color dark red, After The solvent vanished., the precipitated material was filtered out, vacuum-dried, and completely cleaned in ethanol to get rid of any remaining unreacted beginning ingredients (Scheme 1).

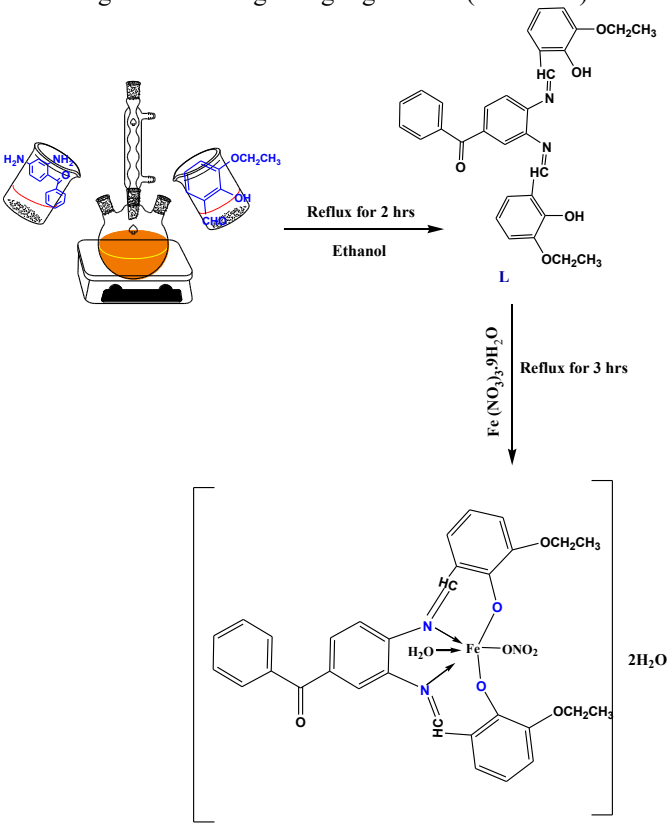

Scheme 1: Synthetic approach to the creation of the FeL complex and imine ligand (L).

2.4. Depiction of the synthesized L imine pro-ligand and its complex

A melting point instrument (Gallenkamp, UK) was used to determine the melting point of the produced imine ligand and the decomposition the complex' degrees. An FTIR-8300 Shimadzu spectrophotometer was used to record the infrared spectra of the KBr pellets. Using a Bruker Avance DPX-500 spectrometer, ^{1}H (nuclear magnetic resonance) and 13 C (nuclear magnetic resonance) spectra were acquired in deuterated dimethylsulfoxide (DMSO) solutions. Using PG spectrophotometer type T + 80- and 10-mm matched quartz cells, all scanning DMF's UV-visible spectrum were noted Cairo University's main laboratory used a PerkinElmer 240c elemental analyzer to perform elemental research. Using Pascal's constants, the diamagnetic corrections were made, and the magnetic susceptibility was evaluated using a Gouy balance. The conductive tester used was a JENWAY 4510 to test the molar conductivity. At various pH ranges, the values of absorption of 5 × 10^{-3} M were ascertained for every compound. Britton universal buffers were used in several tests to determine the pH levels [18]. Using a CL-51B combination electrode, an ADWA AD1000 and AD1020 pH meter was

utilized to detect pH at 298 K. The pH meter was previously calibrated using pH 4.02 and pH 9.18 reference buffers.

2.5. Assessing the prepared imine complex' stoichiometry

The techniques employed were the molar ratio [18, 19] and continuous variation [18–20]. After mixing, agitating, and allowing the ligand and metal salt solutions to equilibrate, the absorbance was measured at λ_{max} for a maximum of two hours. Each solution contained 1×10^{-3} M of metal ions and L imine pro-ligand in total. Ten mixtures from the ligand and metal salt were prepared. The metal salt and L pro-ligand were initially present at 1 mM quantities. Plotting each solution's absorbance against the pro-ligand ([L]/[L] + [M]) or the mole fraction of metal ions was done

2.5.1. Assessment of the produced complex' apparent formation constants

Spectrophotometric measurements were performed using the continuous variation technique to determine manufacturing factors (Kf) of the investigated FeL imine complex under investigation that were produced in solutions. Thinking about the subsequent relationship: [18, 19]

$$K_f = \frac{A/Am}{(1-A/Am)^2 C} \qquad (1)$$

Where A represents the amount of absorption arbitrarily selected on each portion of the absorbance peak, C is the first molar concentration of the metallic element and A_m is the absorption, at the complex's maximum output. Additionally, complex' liberated energy transformation, ΔG*, was ascertained. by ΔG* = -RT ln K, at 25°C, was used to calculate the shift in liberated energy (ΔG) of the complex' synthesis of the metal chelates under examination. T appears to be the specific heat in Kelvin and R is the common gas constant. The formation constant is K_f. (ΔG) of the metal chelate formation that is being examined. It appears that R is the common gas constant, and T is the specific heat in Kelvin.

2.6. Computational details

The Gaussian-09W program was employed for energy minimization examinations while a single crystal X-ray approach was not available for clarifying the geometric structural characteristics.[20] At the B3LYP functional level, the geometrical conformations of the produced compounds were optimized using the DFT technique in the ground condition in the gas state..[21] The B3LYP/6–311G** level was used to optimize the free ligand geometry, and the metal ion basis set (6-311G**-LANL2DZ) was used to optimize the solid Fe chelates structure.[22] All of the bond lengths, dihedral angles, and bond angles were freely released using geometry optimization. Several elements, such as the the geometric parameters are optimized, and The MEP charts in three dimensions, might be studied using the DFT theory. From calculations, the ligand and its Fe chemical reactivity were evaluated, and the quantum chemical variables were clarified.[23] A Gauss View 5[24] program has been used to establish MO illustrations.[25] The nonlinear optical features of the synthesized compounds, namely Δα, μ,<β>, and<α>, were calculated using the x, y, andz ordinates.

2.7. Biological evaluation of the investigated compounds

2.7.1. Antimicrobial properties of the processed substances

The produced chemicals' antimicrobial properties were assessed in opposition to three bacterial strains: *Bacillus subtilis* (+ve), *Staphylococcus aureus* (+ve), and *Escherichia coli* (−ve) the agar well dilution technique [26]. Dimethylsulfoxide (DMSO) was used to dissolve the compounds at concentrations of 10 and 20 mg ml $^{-1}$. Agar with nutrients was made., autoclaved, and then put into sterile Petri plates. The Petri plates with the nutrient agar were allowed to cool before the organisms being studied were cultivated on it. Next, using a sterile cork borer to drill holes in the agar, Whatman paper discs that have been sterilized and soaked with the generated compounds' solution were added. A whole day at 37°C was spent incubating the Petri plates [26, 27]. Comparatively, the conventional medication gentamycin was investigated under comparable circumstances. The negative control, DMSO, proved ineffective against the microbiological pathogens.

2.7.2. Antifungal properties of the compounds that were prepared:

Three fungus strains, *Aspergillus flavus*, *Trichophyton rubrum*, and *Candida albicans*, were used as the environment and the well diffusion method to evaluate the antifungal characteristics of the synthesized ligand and its compounds [26]. The fungi that caused the infection were isolated using the affected sections of the parent plant. The fungus varieties were evenly split into Petri dishes after being combined with potato dextrose agar. The investigated chemicals were placed onto filter paper discs after being dissolved in 10 and 20 mg ml^{-1} DMSO solutions. For 72 hours, these plates were maintained at 35°C in the incubator. The results were displayed as zones of inhibition and compared to the reference medication, fluconazole.

2.7.3. Activities of the produced compounds against cancer:

The test subjects for the pharmaceuticals under study were the Hep-G2 cell line (hepatocellular carcinoma), MCF-7 cell line (breast cancer), and HCT-116 cell line (colon carcinoma), as well as the National Cancer Institute, Cairo University's Pharmacology Department, and the Cancer Biology Department. Every well's absorbance was calculated at 564 nm using an ELISA microplate reader (Σ960, Meter Tech, USA). A 96-multiwell plate was first filled with 104 cells per well, and it was subsequently developed for 24 hours at 37°C. Subsequently, the compounds were put to this plate at varying concentrations in DMSO (0, 1, 2.5, 5 and 10 μM). Thirdly, the plate was incubated in an environment containing 5% CO_2 at 37°C for 48 hours. The plate was then cleaned, dried, and exposed to sulforhodamine B dye staining. The extra stain was removed from the support surface using acetic acid before adding Tris-EDTA buffer. The ELISA reader was employed for evaluation the color magnitude. The following formula was employed to ascertain the concentration of inhibitors. (IC50) [28, 29].

$$(IC)\% \ \frac{(\text{Control OD} - \text{Ligand OD})}{\text{Control OD}} \text{ X } 100 \qquad (2)$$

2.7.4. Antioxidant activities of the prepared compounds:

The color intensity was measured Spectrophotometric ally using PG spectrophotometer. The following formula was used to compute the inhibitory concentration (IC50) [26]. The DPPH absorbance dropped at 517 nm. The same procedure was done

without the tested chemical to find the IC50 and (%) for its capacity to scavenge free radicals [30]. The following formula was used to determine the free radical capture capacity (%):

$$\left(\frac{A_o - A_s}{A_o}\right) \times 100 \quad (3)$$

Where the absorbance of the control and sample are denoted by [Ao] and [As], correspondingly.

Docking of molecules

The docking of molecules was investigated., utilizing MOE2019 software.[31] The Protein Data Bank (PDB) was used to determine the protein crystal structures' ID of Salmonella Typhimurium (PDB ID: 5XHH), Aspergillus flavus (PDB ID: 7WGI), and Colon carcinoma cells (PDB ID: 6GUE). Throughout the several docking simulations using the default parameters, conformational shapes were chosen based on the calculated E conformations values and interaction values, and the flawless binding of the examined chemicals to the corresponding proteins and their amino acids.

3. Results and Discussion:

The L imine pro-ligand's and its compounds' physical-chemical characteristics

The Fe (III) ions in ethanol mix with the L ligand to form the appropriate solid complex. By using elemental analysis, molar conductivity, magnetic susceptibility, IR, UV-Vis, and ^{1}H NMR, the resultant complex was categorized.

3.1. NMR spectra of L imine ligand and its complex

The identification of the compounds was validated by the use of NMR spectroscopy. ^{1}H NMR spectra (Figure 1, S2) and ^{1}H NMR (d, ppm) of the imine L ligand in DMSO-d6:

The ^{1}H NMR spectrum of L imine ligand exhibited singlet signal at δ =12.35, that are assigned to the two phenolic ─OH. group. The signal due to the two azomethine protons (CH═N) is found to be at δ =8.89 ppm. Additionally, it exhibits multiplet signals for aromatic CH (8) protons around 7.78–6.83 ppm. [32, 33]

The L imine ligand's ^{13}C NMR spectra show a signal at 163.7 ppm for the CH=N. Additionally, the signals at 14.3 and 65.4 ppm were appropriate for both aliphatic carbons CH_3, CH_2 collectives Additionally, the signals that show up in the range of 117.9–137.6 ppm are associated with the phenyl carbons, Figure S1.

3.1.2. IR Spectrum

The infrared spectra of L and its complex were found to be between 400 and 4000 cm^{-1} in KBr pellets. By closely comparing the two compounds' infrared spectra, it is feasible to confirm the ligand and metal complex synthesis. These bands include crucial information regarding the composition of the groupings that function that are joined to the metal atoms. The distinctive infrared wavelengths of the L ligand and its complex, together with their associated assignments (Figure S3). The different bands that arise from ─OH and ─CH=N reveal information about the ligand's composition and how it interacts with the metal. The vibration that stretches of C=N is in charge of the band seen in the L ligand at 1611 cm^{-1}.

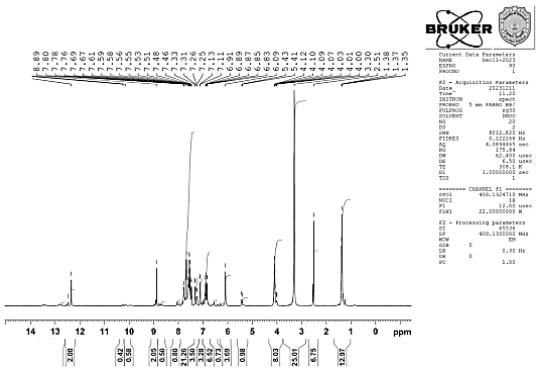

Fig 1:^{1}H NMR and spectra of L imine pro-ligand.

During intricacy, that band moves to a lower frequency (1596). The change in this band indicates unequivocally that azomethine's nitrogen atoms play a role in the production of metal chelates [34].

This is corroborated by the emergence of a ensemble at 430 cm^{-1}, which is the stretching vibration of the M-N bond. Bands at 538 cm^{-1} represent the stretching vibration of M ― O [35]. The band at 3484 cm^{-1} in the ligand spectra is the result of free ―OH stretching vibrations. This band has been shifted to 3364 cm^{-1}, also known as the υ(OH) extending vibration of crystallized water molecules, according to the elemental analysis data. In the produced complex, the group performing at 886 cm^{-1} (OH rocking) suggests the existence of coordinated water. The absorption band in the low-frequency region of the L imine ligand spectrum, located at 1260 cm^{-1}, could perhaps be attributed to the stretching vibration of the phenolic group (C–O). The coordination between the oxygen atoms in the phenolic groups and the metal ion is indicated by the band shifting to reduced values of the wave number (1251) cm^{-1} upon coordination. Three non-degenerated forms can be observed in the distinctive tones of the coordinating nitrate group in the FeL complex.: 1432 cm^{-1} ϋ(NO_2) asy, 1387 cm^{-1} ϋ(NO_2) sy, and 822 cm^{-1} ϋ(NO).

3.1.3. Measurements of electrical conductivity and elemental analysis

The L mine ligand operates as a tetra-dentate and forms complex with Fe (III) ions at a ratio of 1:1 metal to ligand (cf. Scheme 1). The produced imine ligand and its combinations elemental analysis data are mentioned in Table 1.

The resultant complex is not hydrophilic, has a high decomposition point, and is pigmented, hard, and strong at a comfortable temperature. The produced complex' molar conductance was calculated at surrounding temperature using DMF as a solvent; the findings are shown in Table 1 in units of (Ω^{-1} cm^2 mol^{-1}) at ambient temperature, the molar conductivity measurements of the FeL chelate is 11.45 Ω^{-1} cm^2 mol^{-1}, attributed to it, s non-electrolytic character [36, 37].

3.1.4. UV–Vis spectra.

Molecular electronic absorption spectra are frequently necessary for assessing the outcomes of other research techniques.

By analyzing the digital spectra, the characteristics within the ligand region surrounding the metal ion were determined. The ligands' and their complex's electronic absorption spectra were captured at 298 K and in the wavelength range of 800–200 nm.

The molar absorptivity (εmax) and maximum absorption wavelength (λ_{max}) are shown in Figure 2. Two bands are visible in the UV–Vis region about 262,341 nm, which is specified to π→π*, n→π*, [38].

TABLE 1: both physical as well as data from analysis of L imine pro-ligand and its complex.

Compound formula)	(molecular	Molecular weight	Colour	Molar conductance	μeff (BM)	M.p. Dec.temp. (°C)	And	Analysis (%) Found (calcd)	
				$\Lambda_m, \Omega^{-1}cm^2\ mol^{-1}$				C H N	
L	$C_{31}H_{28}N_2O_5$	(508.56)	dark orange	-	-	(170)		73.25.48 (73.[5.89)	5.60 (5.51)
FeL $C_{31}H_{32}FeN_3O_{11}$		(678.44)	blessed	11.45	5.47	>300		54.74.81 (54.[4.71)	6.27 (6.19)

These bands are the result of an intraligand band transition brought on by the activity of the imine and a Transference of charge within molecules transition that occurs in the ligand. Surprisingly, new bands were found at 471 nm and 253 nm, which represent the d-d transition band and π→π*, transition band, respectively [21].

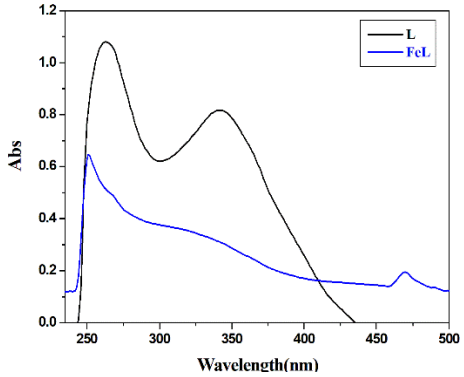

Fig.2. Molecular electronic spectra of L ligand and its FeL complex in ethanol at 298 K.

3.1.5. Moment of magnetism for FeL complex

Studies of magnetic reactivity reveal details on the compounds' geometrical composition. In general, the magnetic moments that is found for complex able to use to diagnose the cooperation geometry surrounding the metal ion (Table 1). The FeL complex has a Magnetic moment which corresponds to five unpaired electrons, or 5.47 BM, as predicted for octahedral Fe (III) chelate.

3.1.6. Mass Spectra

At 250°C and 70 eV, mass spectra were obtained in the electron ionization mode. There is a high connection between the results of the elemental analysis and the detected molecular ion peaks (Figure 3(a,b)). Complex's mass spectra confirm their stoichiometry. The MS spectra of the FeL ligand revealed a molecular ion band at m/z (found (calculated)) = 584.76, whereas the molecular ion band of the imine ligand was around m/z (found (calculated)) = 449.01. These data align with the CHN data. MS of L imine ligand presented a [M+] at m/z = 508 amu that approves the proposed structure [$C_{31}H_{28}N_2O_5$; M. wt = 508.56 g/mol]. MS of FeL chelate presented a [M+] at m/z = 578.46 amu, which is the same as the structure that is suggested. [$C_{31}H_{32}FeN_3O_{11}$; M. wt = 678.44 g/ mol].

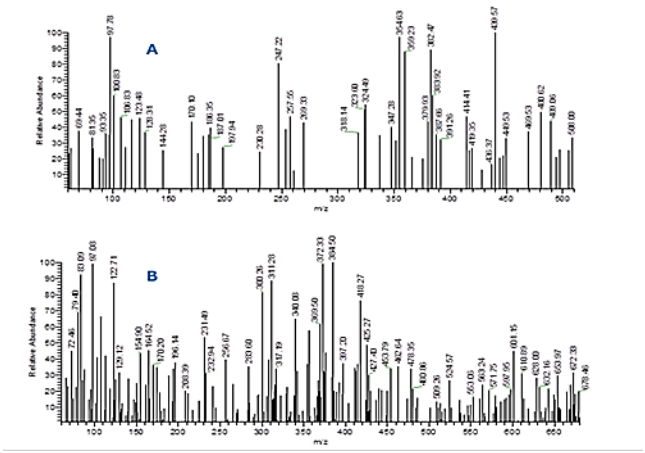

Figure 3: Mass spectrum of the (a) imine ligand L and (b) its FeL complex

3.1.7 Spectrophotometric Measurement of the Prepared Complex's Stoichiometry

The molar ratio approach and the continuous variations method, which both involve spectrophotometry, were employed to ascertain the complex's equilibrium. The produced compounds have a proportionality of 1:1, as indicated by the obtained results. The ongoing change method's curves (Figure 4) exhibit the highest mole fraction absorption X_{ligand} = 0.5–0.6, indicating a 1:1 molar complexation between metal ions and ligand. Furthermore, the produced complex's metal ion to ligand ratio is confirmed by the information derived using the molar ratio method (Fig. S4) [39].

3.1.7.1. Determination the prepared Complex's formation constant.

Using the continuous variation approach, the formation constants (K_f) of the examined imine complex produced in solution were derived from the spectrophotometric data. The tested complex's remarkable stability is demonstrated by the obtained K_f value. For FeL complex in molar ratio (1:1) K_f (5.50×10^5) and ΔG (-32.47) KJ/mol indication the spontaneous reaction of imine ligand L with Fe (III) ion to form FeL complex.

3.1.8. Molecular orbital studies

The most stable geometrical structure was identified by optimizing the ligand structure using the B3LYP/6-311G** of density functional theory level, as shown in Figure 5. The dihedral angle principles in Table S1, which differ from 0 to 180º, indicate the non-planarity of the ligand and focus on its non-coplanar geometric structure. The estimated organic charges on the anticipated chelating sites listed in Table 2 can be used to determine the ligand L chelating centers. Concerning L, the O39, N23, N24, and O57 atoms, the tabulated result shows that their respective natural charges are -0.631, -0.432, -0.523, and -0,661. This underscores the suitability of these atoms as sites of complexation to work in tandem with the Fe metal cations.

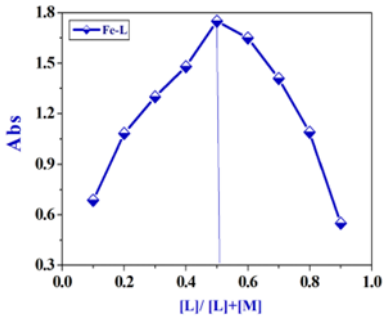

Fig 4: The stoichiometry of the produced compounds in water-based ethanolic solution using Job's plots at 10^{-3} M of [FeL] and 298 K

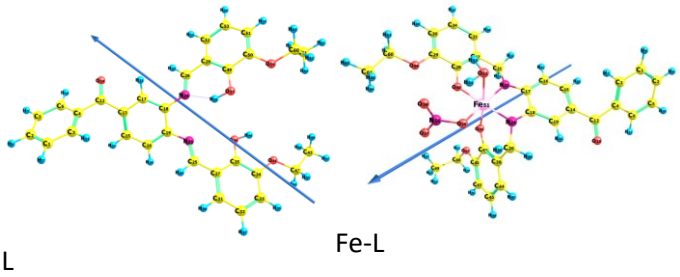

Figure 5. Optimized geometry, bond lengths, numbering system, bond angles, and vector of dipole moment for the studied ligand L and its Fe complex using B3LYP/6-311G** and B3LYP/6-311G**-LANL2DZ level.

Table 2 NBO charges calculated for the ligand L and its FeL complex

Parameter	Ligand L	Fe-L
E_T, eV	-45.81	-58.87
E_{HOMO}, eV	-5.4944	-6.0211
E_{LUMO}, eV	-2.05523	-4.1997
E_g, eV	3.4415	0.8221
I, eV	5.4976	5.0243
A, eV	2.0561	4.2023
χ, eV	3.7768	4.6133
η, eV	1.7207	0.4110
S, eV	0.2906	1.2165
V eV	-3.7768	-4.6133

3.1.8.1 Solid chelates geometry

The B3LYP/6–311G**-LANL2DZ mixed basis sets were applied in order to maximize the ground state geometry of the Fe solid chelate. Figure 5 shows the Fe solid chelate's optimized shape, numbering scheme, and dipole moment vector. The dihedral angle values, bond lengths, and bond angles of the synthesized chelate surrounding the core metal ion are listed in Table S1. The Fe solid chelate C26-N24 and C17-N23 bond lengths are observed to be longer when compared to the ligand. The coordinate bonds formed between the centers of N24 and N23 atoms and metal cations can be attributed to this elongation. However, the bond lengths between O49-C41, and C38-O50 are shortened, suggesting that O49 and O50 are also chelation centers. Metal-nitrogen complex has a longer coordinate covalent bond length than regular M-N bond lengths which decreases the ionic character of the complex.[40] N23, N24, O49, and O50 of the ligand moiety, are the sites of chelation in the Fe-ligand chelate. The distorted octahedral geometry formed by the chelate is indicated by the bond angle values ∠C38-O50-Fe51∠O50-Fe51-N24, ∠Fe51-N24-C26, and ∠O49-Fe51-O50, which are 128.365º, 178.138º, 119.434º, respectively.[41].

3.1.8.2 Global reactivity descriptors

To describe the charge and density of electrons movement in any chemical compound, it is crucial to examine the spatial distribution of molecular orbitals and molecular energy levels. Figure 6 shows the HOMO and LUMO mapping diagrams for the ligand L and its Fe chelate. Determining the redox potentials of the compounds requires knowledge of the HOMO and LUMO energies. In addition, a crucial element in assessing a molecule's chemical reactivity and defining its softness or hardness is the disparity in energy, or Egap, which is the energy distinction between E_{HOMO} and E_{LUMO}. Greater global pliability and chemical responsiveness (S) are the results of easier charge migration and polarization events, which are characterized by smaller energy band gap E_{gap} values; on the other hand, harder and less reactive molecules have larger Egap values. Table 3 displays the results of the computations and collection of total energy, energy gap, electron affinities, E_{gap}= E_{LUMO} - E_{HOMO}, ionization potential, Ip= -E_{HOMO}, Chemical resistance and electrostatic attraction, η = (Ip - A)/2, χ = (Ip + A)/2, chemical potential, V = -(Ip + A)/2, and global softness, S =1/2η.1.

Table 3 Total energy, energy of HOMO and LUMO, energy gap, ionization energy (I), electron affinity (A), absolute electronegativities, (χ), absolute hardness (η), global softness (S) chemical potential (V) of ligand L and its Fe complex using B3LYP/6-311G** and B3LYP/6-311G**-LANL2DZ Level
using B3LYP/6-311G** and B3LYP/6-311G** -LANL2DZ level

	Ligand L	Fe-L
O39	-0.631	-0.576
N23	-0.432	-0.414
N24	-0.523	-0.344
O57	-0,661	-0.471
Fe	-	0.673

The chelation process destabilizes the HOMO of Fe chelate, as evidenced by the ionization potential (Ip) values. The energy of the HOMO is -0.1846 eV when compared to the ligand (-0.2020). However, it was discovered that the chelation process stabilizes the LUMO of FeL chelate. The HOMO is found on the phenyl ring and all oxygen and hydrogen atoms. Except for the two CH_3CH_2O groups, the entire molecule has a distributed LUMO electron density in the ligand. The electron concentration in HOMO is mostly focused on the coordination area of metallic cations, one phenyl ring, and the CH_3CH_2O

group. In the FeL chelate, the LUMO electron density is established throughout the metal cation moiety, except for the three phenyl rings. Table 3 collected reactivity parameters highlight that FeL chelate has a lower energy band gap value than the ligand. This suggests that FeL chelate is highly reactive, with a lower hardness (η) and the highest softness (S) as a result, polarization and charge transfer occur naturally

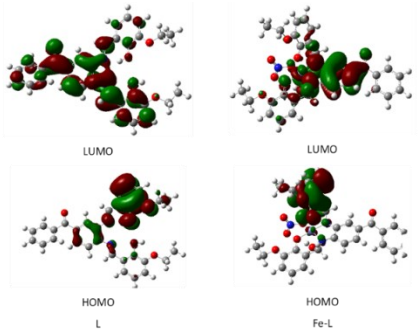

Figure 6. HOMO, and LUMO maps for the studied ligand L and its complex using B3LYP/6-311G** and B3LYP/6-311-LANL2DZ level.

3.1.8.3. Molecular electrostatic potential (MESP)

The Molecular Electrostatic Potential (MEP) is a key property that describes the distribution of electrostatic potential across the surface of a molecule. It provides insights into how a molecule interacts with its environment, particularly in terms of its ability to interact with other molecules (such as proteins, nucleic acids, or small molecules). In the context of biological activity, MEP plays a crucial role in determining how a complex or drug molecule interacts with biological targets, such as enzymes, receptors, or DNA.

Figure 7 shows the 3D maps of electrostatic potential (ESP) and molecular electrostatic potential (MESP) for the ligand L and its investigated Fe chelate. These maps originated from their optimized geometries using B3LYP/6-311G** for the ligand and B3LYP/6-311G**-LANL2DZ for Fe solid chelate. Any molecule's inherent charge transmission and charge on the active locations must be calculated to determine electrophilic or nucleophilic attack.[42] Potential's color scheme is as follows: red < orange < yellow < green < blue.[43] The outcomes show that the negative, or red, area is primarily created over the positions of the nitrogen and oxygen atoms due to the lone pairs of electrons in those atoms participating in Fe chelation. In contrast, blue (positive) potential sites around some hydrogen and carbon atoms. The ligand's N23, N24, and O49, O50 atomic locations' negative potential is verified by the yellow color around those positions. It was observed that the N and O atomic positions in the chelates have the highest negative potential. Conversely, most of the areas that are most favorable are concentrated around hydrogen atoms. An atomic location with negative electrostatic potential is typically the target of an electrophilic attack. Consequently, as the negative potential develops, so does that an electrophilic assault will occur.

3.1.8.4. Naturally population and native charge

Determining the electrical properties of any molecular system greatly depends on the examination of the accumulating debt on its various atomic sites. Table 2 records the atomic natural charges and the natural electronic configuration for the divalent Fe^{3+}, metal ion. The calculations showed that the metal ion charges are smaller than its formal (3+) charge because of the ligand's N23, N24, and O49, O57 atoms' electrons being electron donating. As seen in Table 2, the atoms N23, N24, O39, and O57 have the highest concentration of negatively charged atomic sites, making them the ligand's electron-donating sites. However, it was found that the Fe metal ion had a lower electropositive charge of 0.673 which can be attributed to the Fe metal's d^6 orbital. The metal ions in the FeL chelate have received 2.327e ($3d^{6.60}$), from the ligand donating sites, according to **Table S2**'s data.

3.1.8.5. Non-linear optical characteristics (NLO)

The dispersal of charges of atoms is very helpful in determining the direction and size of their moment. Due to their widespread use in optical information, optical computing, and optical data storage processing, NLO compounds have attracted much attention.[44] Table 4 lists the ligand's L polarizabilities, hyperpolarizabilities, and total static dipole moment under study, its Fe chelate, and the experimental approximation of urea, based on the similarity degree of the applied theory. The model NLO experimental prototype chosen was urea.[45] Since the considered compounds' NLO characteristics lacked experimental values, urea was used as a point of comparison. The results gained are not reliable with earlier research that can be in the literature.[46] The polarizabilities and first-order hyperpolarizabilities were expressed in atomic units (au). A conversion ratio was used to multiply the values that were obtained. of 8.6393x10-33 esu for (β) values and $0.1482x10^{-24}$ esu for (α) values. Table 4's data indicates that all the ligand and its Fe complex are polar, as stated by their dipole moment (μ) values. As a result, their polarity is arranged in the following order: FeL > Ligand and their dipole moments are all greater than urea. The NLO system's first-order hyperpolarizability parameter is regarded as one of its most important features. The β parameter's range shows that the ligand is around eighteen times higher than urea, whereas the chelates FeL is seven times higher than urea. As a result, the ligand and its Fe chelate is excellent choices for NLO materials.

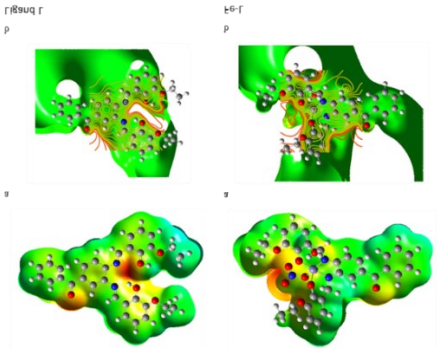

Figure 7: Potential electrostatic between molecules (a) and contours electrostatic potential surfaces (b) of the studied ligand L and its complex using B3LYP//6-311G** and B3LYP//6-311G**-LANL2DZ level.

Table 4. Calculated total static dipole moment (μ), the mean polarizability<α>, anisotropy of the polarizability Δα, and the first-order hyperpolarizability<β>configuration for the studied ligand L and its Fe complex using B3LYP/6-311G** and B3LYP/6-311G**-LANL2DZ level

Property	Urea	Ligand L	Fe-L
μ, D	1.3197	5.81	6.34
αxx, a.u.	-	-164.158	-236.7692
αyy	-	-195.988	-227.0299
αzz	-	-224.8947	-260.4688
αxy	-	10.6103	-12.2317
αxz	-	-2.72	-8.0838
αyz	-	-5.2388	2.7376
<α>esu	-	-2.8901×10^{-23}	-3.5779×10^{-23}
Δα, esu	-	7.7983×10^{-24}	4.4146×10^{-24}
βxxx	-	201.0708	92.3356
βxxy	-	-133.5364	-169.274
βxyy	-	152.6718	-113.8876
βyyy	-	-13.524	63.5929
βxxz	-	13.691	93.1998
βxyz	-	33.7465	-43.1498
βyyz	-	19.9151	40.7506
βxzz	-	20.5408	-44.5671
βyzz	-	-0.3432	32.3141
βzzz	-	0.0403	-11.7047
<β>, esu	0.1947×10^{-30}	3.4874×10^{-30}	1.3577×10^{-30}

3. 2. pH profile

As seen in Figure 8, the complex's pH profiles display distinctive dissociation curves. From pH 4 to 10, these compounds show a wide stability range. This broad stability range suggests that when the ligand is unbound, the pairings are more secure. over a wider range of pH. As a result, this complex show no degradation or loss of functionality and can be used in a variety of applications in the pH range of 4 to 10 [46].

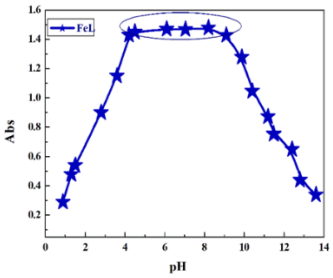

Figure 8: The stability behaviour of the inspected FeL complex at different pH media

3.3. Assessment of the effectiveness of anti-microbial medications

Numerous fungi and bacteria were tested against the L ligand and its combination. The efficiency of these medications was assessed using the calculated zone of inhibition (mm) (Table S3, Figs. 9 and 10), minimum inhibitory concentration (MIC, mg/mL) (Table 5), and activity index (Table S4). The investigated FeL complex had an encouraging antibacterial activity when compared to the free ligand and the reference drug [47]. Reduced minimum inhibitory concentrations, a high activity index percentage, and a wide inhibition zone are necessary for this outcome. It was previously shown that chelation theory can be used to investigate and fully predict metal chelate activity. Metal ions increase toxicity to a desirable level due to the degree to which their positive charges are decreased after coordination. This reduction facilitates the interaction and penetration of cell membranes by biological systems by enhancing lipophilicity. A comparison of anti-bacterial activity of the inspected compounds with other compounds in literature were reported in Table S3 [48]. The following relationship was used to calculate the potency index (Table S4) in order to validate the effects of the synthetic chemicals:

$$\text{Activity index} \frac{\text{Inhibition zone of complex (mm)}}{\text{Inhibition zone of standard drug (mm)}}\times100$$

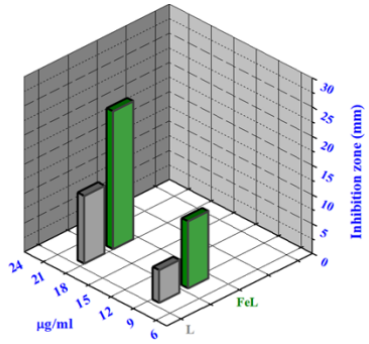

Fig 9: Histogram comparing the produced compounds' antibacterial activity (L and FeL) against *Escherichia Coli (-ve)*

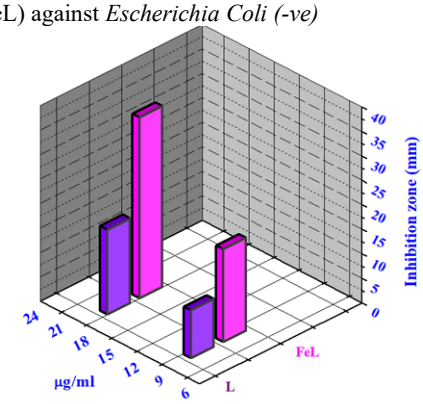

Fig 10 Histogram comparing the produced compounds' antifungal activity in comparison (L and FeL) against Getrichm Candidum

Table 5: Minimum inhibition zone (MIC) for antimicrobial assay of the prepared **L** ligand and its metal chelates

compounds	bacteria					Fungi
	S. Typhimurium (-ve)	*E. Coli (-ve)*	*B. Cereus (+ve)*	*A. Flavus*	*G. Candidum*	*F. Oxysporum*
L	**7.50**	**7.75**	**6.50**	**7.50**	**5.75**	**7.00**
FeL	**4.75**	**5.50**	**4.00**	**5.75**	**4.50**	**5.25**

The differences in metal complex action against different bacteria are due to differences in the ribosomes of the microbial cells or the impermeability of the microbes' cells. The reduced activity of

complexes relative to others could be due to limited lipid solubility, preventing the metal ion from reaching the cell wall's favorable site of action and interfering with normal cell activity.

3.4. Anticancer activity

The ligand and its complex, a produced L imine, were evaluated for their cytotoxic ability opposing colon cancer in humans' cells (HCT-116 cell line), hepatic cellular carcinoma cells (HepG–2), and breast cancer cells (MCF-7 cell line) at concentrations between 0 and 10µM. The IC50 values were computed for each medication, and the results are displayed in Table S5 and Fig. 11. The observations indicate a potential inhibitory feature for the tumor cell proliferation under investigation, FeL, when compared to the medicine vinblastine. The unique Complex's capacity to bind negatively charged DNA on tumor cells is the main factor driving its cytotoxic effect. This damage to the DNA structure ultimately resulted in the suppression of transcription and replication, as well as the death of the cell [49]. Two of the many pathways that lead to cell death caused by cytotoxic substances are necrosis and apoptosis. Cell shrinkage, chromatin condensation, and plasma membrane hemorrhage are signs of apoptosis [50]. A comparison of anti-cancer activity of the inspected compounds with other related studies were reported in Table S5 [51, 52]

3.5. Antioxidant activity

A conscious attempt to combat free radicals was taken into consideration because it is well known that they play a significant role in infection. The DPPH test was utilized to evaluate the ligand and its characteristics. It is noteworthy that oxidative processes involving free radicals play a pathologically important role in the aging process and the development of numerous human disorders [53]. The in vitro antioxidant activity of L and its metal chelate was evaluated using the useful method of DPPH. The evaluated compounds were generated in different concentrations (10, 25, 50, 100, and 150 µg/mL) to compare their antioxidant ability with that of ascorbic acid, a common treatment. The acquired findings (Fig. 12), (Table S6) demonstrated that FeL complex has more antioxidant activity than the free ligand. FeL exhibits significant antioxidant activity, as seen by its ascorbic acid-like IC50 value of 31 µg/mL.

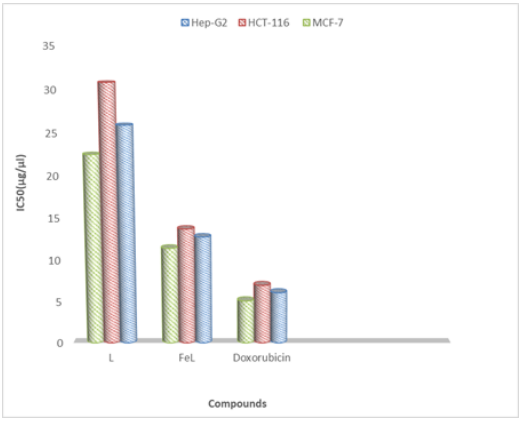

Fig 11 L imine ligand and its complex' IC50 values against the HCT-116, HepG-02, and MCF-7 cell lines

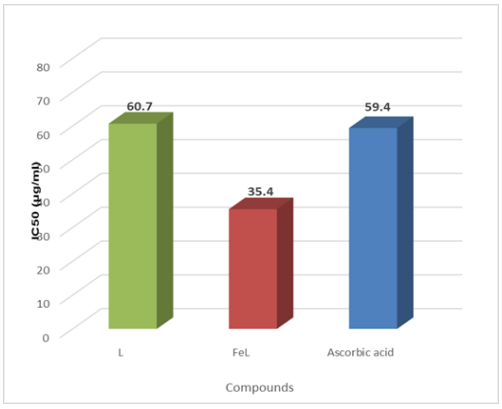

Fig. 12. The L ligand and its FeL complex inhibitory characteristic towards DPPH radical

3.6 Molecular docking on antimicrobial and anti-colon activity

Molecular docking studies validated the inhibitor's potency. The inhibition of cell wall production, protein synthesis, nucleic acid (DNA) synthesis, and anti-metabolism are typically included in the mechanism of action of anti-bacterial drugs [54.] The binding pocket residues of the bacteria were chosen from PDB to examine their pattern of binding with respect to the target protein based on the experimental results of bacterial and colon cancer activity. All the prepared compounds were docked with two different microorganisms *Salmonella Typhimurium*, (PDB ID: 5XHH) and *Aspergillus flavus* (PDB ID: 7WGI), and Colon carcinoma cells (PDB ID: 6GUE). They were examined for binding free energy and their interactions with the protein receptor. The docking data are shown in Table S7, which also offers an impression of the binding energy interaction in Kcal/mole between the obtained compounds and bacterial protein receptors. The 2D and 3D representations of docking interactions for all bacteria, and colon cancer cells are revealed in Figure 13, where dashed lines represent hydrogen bonds. It was noticed that the created compounds' binding interaction surfaces with bacterial protein receptors were made up of hydrogen acceptor, and pi-hydrogen. These assemblies demonstrated good stability in conjunction with hydrogen bonding in docking compounds. [21(a)] The strength of the interaction between the selected proteins and the substances being tested is tracked and recorded in Table S7, simulating the genuine docking cycle. Proteins mostly bind to the chemicals under investigation via pi-hydrogen or hydrogen acceptor. The negative binding affinities show how widely these processes have happened. The materials under test exhibit a stronger binding affinity to the protein receptor when their binding energy decreases. The data in Table 1 showed that the ligand L has a binding energy score that is more negative with the 6GUE protein receptor. The binding affinity of L-6GUE is greater than that of Fe-L-6GUE chelate, demonstrating the increased inhibition effect of L-6GUE against Colon carcinoma cells (PDB ID: 6GUE). The binding affinity for the established Fe opposes the protein receptor with compounds was observed to be in order Fe-L-6GUE>Fe-L-7WGI>Fe-L-5XHH.

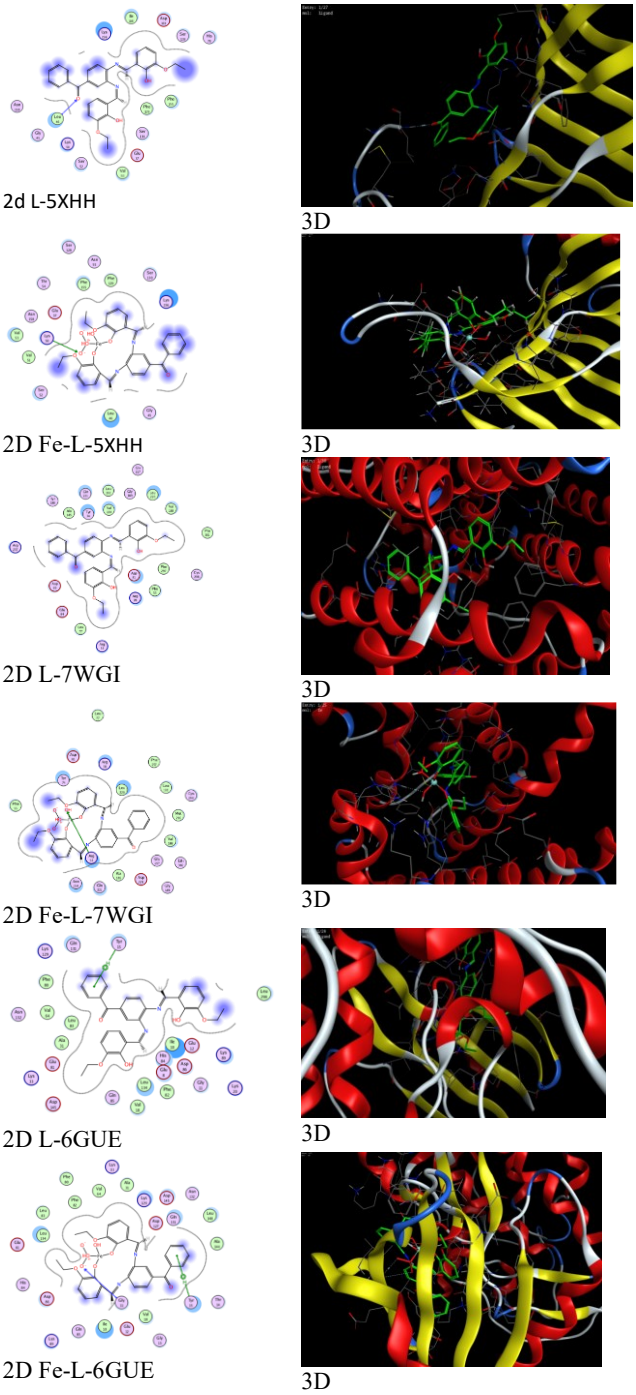

Figure 13. Molecular docking simulation studies of the interaction between the investigated ligand L and its Fe complex with the active site of the receptor of Salmonella Typhimurium (PDB ID: 5XHH), Aspergillus Flavus (PDB ID: 7WGI), and Colon carcinoma cells (PDB ID: 6GUE).

Conclusion

{3,4-Bis-[(3-ethoxy-2-hydroxy-benzylidene)-amino]-phenyl}-phenyl-methanone (L ligand) was employed to get ready novel Fe (III) coordination chelate. Numerous analytical and spectroscopic methods, such as elemental (CHN) analysis, molar conductance, (IR) spectroscopy, (^{1}H & ^{13}C) nuclear magnetic resonance (NMR) spectroscopy, and UV–visible spectroscopy, have been used to classify and examine this recently produced compound. The outcomes of these methods yielded important details regarding the complex's chemical formulas. According to studies in solution data, the (L) ligand coordinates with the chosen metal in a neutral tetra-dentate mode with a stoichiometric ratio of 1:1 (M: L). The 1:1 molar ratio was validated when the chelation behavior was investigated in solution using reference techniques. It was discovered that the compounds were stable across a large pH range (4–10).

Studies on conformation were carried out to clarify the complex's preferred forms. Conformational studies were conducted to elucidate the preferred structures of the complexes. Additionally, the antimicrobial efficiency of the tested complexes was evaluated, and they displayed good anti-pathogenic activity. Furthermore, the complexes exhibited promising cytotoxicity versus three cancer cell lines, particularly (MCF-7). To further validate the findings, in silico tests have been applied using DFT approach and molecular docking. The data from the in-silico studies were acquired to be in well matching with the experimental examinations. In conclusion, tetra-dentate azomethine ligand-based iron (III) complex has a great deal of promise for use in biomedical settings, particularly in the fields of drug delivery, MRI imaging, enzyme mimetics, anticancer therapy, and antibiotic therapy. Nevertheless, more investigation is required to address issues with toxicity, stability, and targeted distribution so that their full promise can be achieved in practice.

CRediT authorship contribution statement

Conceptualization, Ahmed M. Abu-Dief; methodology, Mona M. A. Alharas; Ahmed M. Abu-Dief software, Ahmed M. Abu-Dief; validation, Ahmed M. Abu-Dief, Samir A. Abdel-Latif and Mona M. A. Alharas; formal analysis, Mona M. A. Alharas; Ahmed M. Abu-Dief investigation, Ahmed M. Abu-Dief, Samir A. Abdel-Latif and Mona M. A. Alharas; resources, Rafat M. El-Khatib; Mona M. A. Alharas data curation, Mona M. A. Alharas; writing—original draft preparation, Ahmed M. Abu-Dief, Samir A. Abdel-Latif and Mona M. A. Alharas; writing—review and editing, Ahmed M. Abu-Dief and Samir A. Abdel-Latif; visualization, Samir A. Abdel-Latif and Ahmed M. Abu-Dief; supervision, Rafat M. El-Khatib and Ahmed M. Abu-Dief; project administration, Ahmed M. Abu-Dief; funding acquisition, Rafat M. El-Khatib and Ahmed M. Abu-Dief; All authors have read and agreed to the published version of the manuscript.

Data availability statement

The data used to support the findings of this study are available from the corresponding author upon request.

Declaration of competing interest

The authors declare that they have no known competing financial interests or personal relationships that could have appeared to influence the work reported in this paper.

References

[1] S. Kundu, A.K. Pramanik, A.S. Mondal, T.K. Mondal, *Journal of molecular structure,* 1116 (2016) 1–8.

[2] A.A. Abdel Aziz, A.N.M. Salem, M.A. Sayed, M.M. Aboaly, *Journal of molecular structure,* 1010 (2012) 130–138.

[3] Z.L. You, H.L. Zhu, W.S. Liu, *Z. Anorg Allg Chem.* 630 (2004) 1617; (b) S.S. Hassan, N.M.H. Rizk, M.A. Khidr, S.A. Aly, *Applied Organometallic Chemistry,* 38(1), (2024) e7298.

[4] A. Golcu,M.Tumer, H. Demirelli, R.A. Wheatley, *Inorg. Chim. Acta,* 358 (2005) 1785.

[5] K.T. Samina, A.Y. Abhijit, S.B. Ratnamala, *Journal of molecular structure,* 1152 (2018) 223–231.

[6] R.C. Maurya, P. Patel, S. Rajput, *Synthesis and Reactivity in Inorganic and Metal-Organic Chemistry,* 33 (2003) 817–836.

[7] U. Bohme, B. Gunther, *Inorganic Chemistry Communication,* 10 (2007) 482–484.

[8] L.C. Felton, J.H. Brewer, *Science,* 105 (1947) 409–410.

[9] K.N. Kumar, R. Ramesh, *Polyhedron,* 24 (2005) 1885–1892.

[10] A.N. Kursunlu, E. Guler, F. Sevgi, B. Ozkalp, *Journal of molecular structure,* 1048 (2013) 476–481.

[11] S.P. Fricker, *Dalton Transactions,* 43 (2007) 4903–4917.

[12] R.R. Crichton, D.T. Dexter, R.J. Ward, *Coord. Chem. Rev.,* 252 (2008) 1189 1199.

[13] R. Cini, G. Tamasi, S. Defazio, M.B. Hursthouse, *Journal of Inorganic Biochemistry,* 101 (2007) 1140–1152.

[14] A. Rauf, S. Afzal, S.M. Khurram, K. Abdul Aziz, A. Rashda, A.Y. Muhammad, M.K. Asad, K. Abdur Rahman, Z.Q. Irfan, K. Heinz-Bernhard, Zia-ur-R, *Journal of molecular structure,* 1145 (2017) 132–140.

[15] Z.H. Chohan, M. Praveen, A. Ghaffer, *Synth. React. Inorg. Met.,* 28 (1998) 1673–1687.

[16] G.Y. Nagesh, B.H.M., *Journal of molecular structure,* 1085 (2015) 198–206.

[17] H.S. Calık, E. Ispir, S. Karabuga, M. Aslantas, *Journal of Organometallic Chemistry,* 801 (2016) 122–129.

[18] L.H. Abdel-Rahman, A.M. Abu-Dief, R.M. El-Khatib, S.M. Abdel-Fatah. *Bioorganic Chemistry,* 69, 140.

[19] L.H. Abdel-Rahman, R.M. El-Khatib, L.A.E. Nassr, A.M. Abu-Dief, M. Ismael, A.S. Amin, *Spectrochimica Acta,* 117 (2014) 366–378.

[20] M.J. Frisch, G.W. Trucks, H.B. Schlegel, G.E. Scuseria, M.A. Robb, J.R. Cheese-man, et.al., Gaussian 09W, Revision A.1, *Gaussian Inc., Wallingford,* CT, 2009.

[21] A. D. Becke, *Journal of Chemical Physics,* 1993, 98, 5648.

[22] M. J. Frisch, J. A. Pople and J. S. Binkley *Journal of Chemical Physics,* 1984, 80, 3265.

[23](N. A. El Ghamaz, M. A. Diab, A. A. El Bindary, A. Z. El-Sonbati and H. A. Seyam, *Mater. Sci. Semiconductor Process, 27* (2014) 521

[24] R. Dennington, T. Keith and J. Millam, Gauss View, Version 5, Semichem. Inc., K. S. Shawnee Mission, 2009.

[25] D. Avci, *Spectrochimica. Acta,* Part A, 82(2011) 37.

[26] M. Tyagi, S. Chandra, P. Tyagi, *Spectrochim. Acta,* A 117 (2014) 1–8.

[27] W. H. Mahmoud, R. G. Deghadi& G. G. Mohamed, *Applied Organometallic Chemistry,* 32(4), (2018) e4289.

[28] W. H. Mahmoud, R. G. Deghadi, & G. G. Mohamed, *Applied Organometallic Chemistry,* 32(4), (2018) e4289.

[29] S. S. Hindo, M. Frezza, D. Tomco, M.J. Heeg, L. Hryhorczuk, B. R. McGarvey &C.N. Verani, *European journal of medicinal chemistry,* 44(11), (2009) 4353-4361.

[30] M. I. Hossain, M. Świtalska, W. Peng, M. Takashima, N. Wang, M. Kaiser, & Inokuchi, *European journal of medicinal chemistry*, 69, (2013) 294-309.

[31] F. A. Saad, N. M. El-Metwaly, M. S. Refat, & A. M. Khedr, *Russian Journal of General Chemistry,* 88, (2018) 1258-1265.

[32] Molecular Operating Environment (MOE), 2019.01, Chemical Computing Group ULC, Montreal, QC, Canada, 2019.

[33] H. Uh, P. D. Badger, S. J. Geib, S. Petoud, *Helvetica Chimica Acta,* 92(11), (2009) 2313-2329.

[34] I. Kaya, & A. Aydın, *Polymers for Advanced Technologies*, 22(6), (2011) 951-961.

[35] A. Ourari, K. Ouari, M. A. Khan, & G. Bouet, *Journal of Coordination Chemistry*, 61(23), (2008) 3846-3859.

[36] A. A. Emara,*Spectrochimica Acta* Part A: Molecular and Biomolecular Spectroscopy, 77(1), (2010) 117-125.

[37] W. J. Geary, *Coordination Chemistry Reviews,* 7(1), (1971)81-122.

[38] S. Chandra, S. Raizada, M. Tyagi, & P. k. Sharma, *Spectrochimica Acta* Part A: Molecular and Biomolecular Spectroscopy, 69(3), (2008) 816-821.

[39] E. Pahontu, I. Usataia, V. Graur, Y. Chumakov, P. Petrenko, V. Gudumac, A. Gulea, *Appllied Organometallic Chemistry*, 32 (12) (2018) e4544.

[40] L. H. Abdel-Rahman, A. M. Abu-Dief, Hamdan, S. K.,&Seleem, A. A. *International Journal of Nanomaterials. and Chemistry,* 1(2), (2015) 65-77.

[41] A. Z. El-Sonbati, M. A. Diab, A. A. El Bindary, M. I. Abou Dobara and H. A. Seyam, *Journal of Molecular Liquid* 218 (2016) 434.

[42] S. S. Zumdahl, Chemistry for Chemical and Biological Sciences, University Science Books, Sausalito, CA, 2000.
[43] J. S. Murray and K. Sen, Molecular Electrostatic Potentials, Concepts and Applications, Elsevier, Amsterdam 1996.
[44] P. Politzer and J. S. Murray, *Theor. Chem. Acc.,* 108 (2002)134.
[45] D. S. Bradshaw and D. L. Andrews, *J. Nonlinear Opt. Phys. Mater.*, 18 (2009)285.
[46] L. H. Abdel-Rahman, M. S. Adam, A. M. Abu-Dief, H. E. Ahmed, A. Nafady, *Molecules*, 25, (2020)5089.
[47] A. Arunadevi, & N. Raman, *Applied Organometallic Chemistry,* 32(4), (2018) e4250.
[48] N. G. Fahad, N. H. Imran, Hussein Ali Kadhim Kyhoiesh, Mohammed K. Al-Hussainawy, Results in Chemistry, 6, (2023) 101049
[49] C.R. Vinodkumar, M.K.M. Nair, P.K. Radhakrishnan, *Journal of Thermal Analysis and Calorimetry,* 61 (2002) 143
[50] K. Siddappa, S.B. Mane, D. Manikprabhu, *Science World Journal,* 2014 (2014) 817365
[51] H. A. K. Kyhoiesh , K. J. Al-Adilee, *Inorganica Chimica Acta,* 55, (2023) 121598
[52] H. A. Kadhim Kyhoiesh, K. J. Al-Adilee, *Results in Chemistry*, 3 (2021)100245.
[53] L.H. Abdel-Rahman, R.M. El-Khatib, L.A.E. Nassr, A.M. Abu-Dief, *Arabian Journal of Chemistry,* 10, (2017) S1835
[54] M. Hussain, T. Qadri, Z. Hussain, A. Saeed, P. A. Channar, S. A. Shehzadi, M. Hassan, F. A. Larik, T. Mahmood, A. Malik,, *Heliyon* 5.11 (2019): e02812.